ACS OMEGA

Open Access

http://pubs.acs.org/journal/acsodf

Article

Al@SiO_2 Core–Shell Fillers Enhance Dielectric Properties of Silicone Composites

Bin Huang, Yan Yu, Yan Zhao, Yunfeng Zhao, Lina Dai, Zhijie Zhang,* and Hua-Feng Fei*

Cite This: *ACS Omega* 2023, 8, 35275−35282

Read Online

ACCESS | Metrics & More | Article Recommendations | Supporting Information

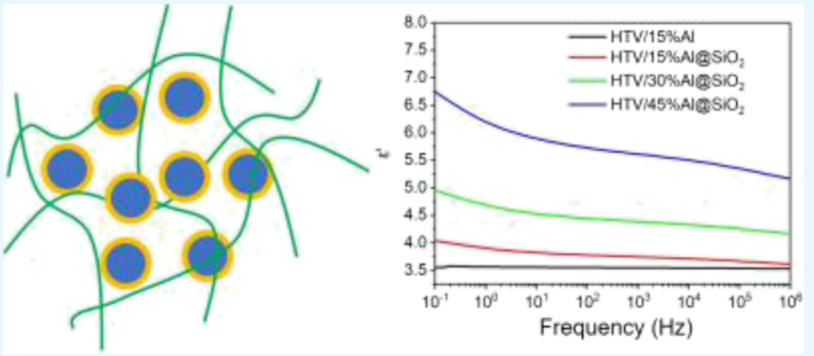

ABSTRACT: Over the past decade, there has been significant interest in polysiloxane-based dielectric elastomers as promising soft electroactive materials. Nevertheless, the natural low permittivity of polydimethylsiloxane has limited its practical applications. In this study, we have developed silicone rubber/Al@SiO_2 composites with a high dielectric constant, low dielectric loss, and high electrical breakdown strength by controlling the shell layer thickness and the content of the core–shell filler. We also investigated the dielectric behavior of the composites. The use of core–shell fillers has increased the Maxwell–Wagner–Sillars (MWS) relaxation process while reducing the dielectric loss of direct current conductance in silicone rubber composites. Moreover, the temperature dependence of the MWS relaxation time in the composites follows the Arrhenius equation. This strategy of increasing the permittivity of silicone composites through core–shell structural fillers can inspire the preparation of other high dielectric constant composites.

1. INTRODUCTION

Dielectric elastomers are composed of an elastomer film that is situated between two electrodes that are thin and flexible. This results in a capacitor that can transform electrical energy into mechanical energy.[1] Dielectric elastomers have attracted growing research interest due to their numerous benefits, including high mechanical strength, low weight, affordability, quick response, high strain, excellent flexibility, and high energy density. As a result, they are ideal for use in actuators, generators, and sensors.[2−4] Silicone rubber is one of the most commonly used materials for dielectric elastomer actuators due to its wide temperature range, good weather resistance, high efficiency, low toxicity, good shear stability, and insensitivity to air humidity.[5,6] However, the applications of silicone rubber are limited due to its low dielectric constant (2.5−3.0@1 kHz).[7,8] To enhance the dielectric constant of silicone rubbers used in dielectric elastomers, researchers have employed several methods, including chemical modification of polysiloxane,[9−11] incorporation of high dielectric constant inorganic nanofillers into the silicone rubber matrix,[12−16] and adding conductive nanofillers to the matrix of silicone rubber.[17−19] However, chemical modification involves cumbersome synthesis steps, high cost, and reduces the temperature range of the polymer.[20,21] When inorganic fillers are added to silicone rubber to increase its dielectric constant, there is a trade-off in the form of an increase in the elastic modulus, which is detrimental to the actuating performance of the material.[22] Incorporating conductive fillers into silicone rubber below the percolation threshold can significantly improve the composite's dielectric constant without compromising the rubber's elasticity.[23] Nevertheless, such composites are prone to leakage currents, which can cause a marked rise in dielectric loss and a reduction in the electrical breakdown strength (E_b) of the silicone rubber.[24]

To reduce the adverse effects of conductive fillers on the E_b and the dielectric loss of the composites, core–shell fillers have been used, which contain insulating materials covered with

Received: July 14, 2023
Accepted: September 7, 2023
Published: September 14, 2023

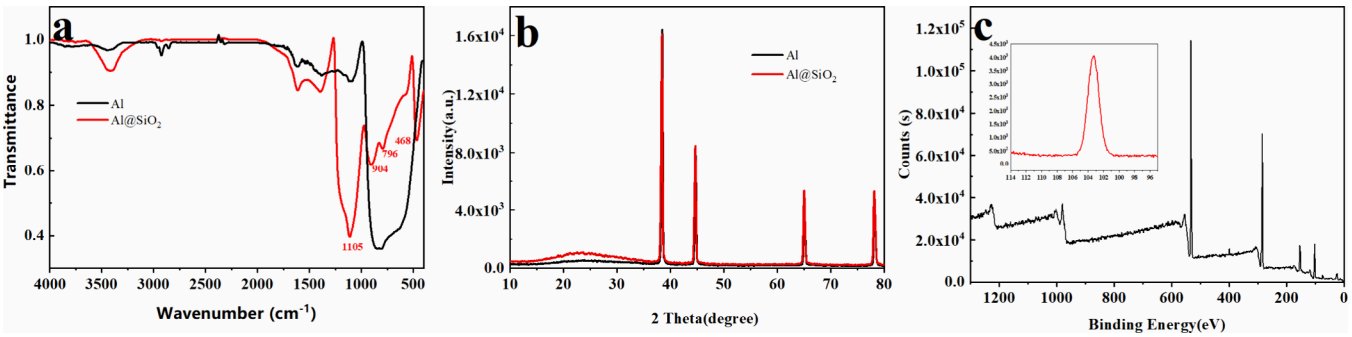

Figure 1. (a) FTIR, (b) XRD, and (c) XPS characterization results for $Al@SiO_2$.

conductive fillers.[25] Typically, the presence of an insulating shell layer can hinder the generation of the conducting network, improve phase interface, and provide a buffer.[26] In addition, the insulating layer effectively reduces the leakage current, electric field concentration, and tunneling current.[27] These factors help overcome the contradictory low E_b and high dielectric loss observed in nanocomposites with high dielectric constants. Quinsaat et al. reported an $Ag@SiO_2$ core−shell filler and compounded it with polydimethylsiloxane (PDMS) to prepare a dielectric elastomer and obtained high tensile, high flexibility, high dielectric constant, low dielectric loss, and high thermal stability of the actuator.[28] However, metallic silver is expensive and cannot be produced cheaply on a large scale. Zhang et al. introduced a $CNT@Al_2O_3$ core−shell filler to prepare a new dielectric elastomer with excellent dielectric properties.[29] However, because the interfacial interaction between the insulating Al_2O_3 shell layer and the silicone rubber substrate is much weaker than that of SiO_2 with silicone rubber, the $CNT@Al_2O_3$ core−shell filler-based dielectric elastomer has very poor mechanical properties.

In this work, we prepared functional filler $Al@SiO_2$ with the aluminum and silica act as core and shell, respectively, and further enhance the dielectric properties of silicone/$Al@SiO_2$ composites by tuning the shell layer thickness of the core−shell filler. The effects of the presence or absence of the shell layer and the core−shell filler content on the composites' dielectric properties were investigated. The composites with a core−shell filler were found to exhibit excellent dielectric properties compared to the composites with pure aluminum powder. Furthermore, we examined the impact of temperature on the dielectric characteristics and dielectric relaxation behavior of the composites using broadband dielectric spectroscopy (BDS) and the Havriliak−Negami (HN) equation. We discovered that the $Al@SiO_2$ core−shell filler, which we synthesized, greatly improved the MWS relaxation while mitigating the impact of their DC conductance on the composites.

2. EXPERIMENTAL PROCEDURES

2.1. Materials. Jiangxi Xinghuo Silicones Co., Ltd. (China) supplied the Methyl vinyl silicone rubber (VMQ). Di-*tert*-butyl 1,1,4,4-tetramethyltetramethylene diperoxide (DBPMH, 92%) was provided from J&K Chemical Co., Ltd. Beijing Chemical Works (China) provided tetraethyl orthosilicate (TEOS) and ammonium hydroxide (NH_4OH, purity is 25−28%). Beijing Deke Daojin Science and Technology Co., Ltd. (China) supplied the aluminum nanopowder (Al, 50 nm).

2.2. Preparation the Core−Shell Filler of $Al@SiO_2$. The aluminum nanopowder was dispersed in anhydrous ethanol by ultrasonication.[30] Then, TEOS, NH_4OH, and deionized water were added dropwise during sonication. The reaction temperature was controlled at 40 °C, and after 6 h of allowing the reaction to reach completion, the samples were extracted, washed, and then dried in an electrothermal blowing drybox for 12 h to obtain the $Al@SiO_2$ core−shell filler. The powder was ground with a mortar and pestle until the particles were homogeneous and then stored for use. By adjusting the feeding ratio of TEOS and aluminum nano powder, the $Al@SiO_2$ core−shell filler with different thicknesses was obtained.

2.3. Preparation the Composites of Silicone/$Al@SiO_2$. Preparation of HTV (high-temperature vulcanized silicon Rubber)/$Al@SiO_2$ composites: The process involved mixing VMQ raw rubber with the curing agent DBPMH and varying the ratios of the $Al@SiO_2$ core−shell filler. The materials were well mixed with double rollers, then pressed into the mold, raise the temperature to 170 °C and maintain 10 MPa pressure, crosslink for 10 min. Then, the composites were demolded and postcured under 200 °C for another 4 h. The composites were identified as HTV/15% $Al@SiO_2$, HTV/30% $Al@SiO_2$, HTV/45% $Al@SiO_2$, HTV/100% $Al@SiO_2$, and HTV/150% $Al@SiO_2$, based on the mass fraction of $Al@SiO_2$ core−shell filler. The HTV/Al composites were prepared by a similar method.

2.4. Characterization. The German Novocontrol dielectric impedance spectrometer was utilized to conduct the BDS at temperatures spanning from −140 to 150 °C and a frequency spectrum of 10^{-1}−10^6 Hz. The frequency analyzer is integrated into the impedance spectrometer, while the use of Quatro cryogenic system units ensures precise temperature control for high accuracy and repeatability. The samples were sandwiched between copper plate electrodes and measured under a dry N_2 atmosphere. The cylindrical samples had dimensions of 2 cm in diameter and 0.03 cm in height. To test the electrical breakdown strength, samples (dimensions were 5 cm × 5 cm × 0.03 cm) were tested in silicone oil at room temperature using a direct current dielectric strength tester. FT-IR analysis was performed using a Bruker Hong Kong Limited Tensor 27 Fourier transform infrared spectrometer. The XRD was measured on a Rigaku D/max 2500 polycrystalline X-ray diffractometer from Japan, while the XPS was conducted using an ESCALab 250Xi multifunctional XPS from VG in the United States. The JEM-1011 and JEM-2100F transmission electron microscopes from JEOL in Japan were applied to characterize the morphologies and elemental analysis of the core−shell particles. The Instron 5565 from British Instron Ltd. was used to measure mechanical properties at room temperature, with five dumbbell-shaped samples tested for each sample group.

https://doi.org/10.1021/acsomega.3c05066
ACS Omega 2023, 8, 35275−35282

3. RESULTS AND DISCUSSION

3.1. Characterization of Core−Shell Fillers Al@SiO_2. Figure 1a displays the FT-IR spectroscopy of aluminum and Al@SiO_2, which reveals the characteristic peak of Si−O−Si at 468 cm^{-1}, the symmetric stretching vibration peak of Si−O−Si at 796 cm^{-1}, the stretching vibration absorption peak of the Si−O bond at 904 cm^{-1}, and the strong and broad absorption band at 1105 cm^{-1}, which corresponds to the antisymmetric stretching absorption peak of Si−O−Si. These FT-IR results provide evidence that the SiO_2 shell was effectively synthesized.

Figure 1b shows the XRD spectra of Al and Al@SiO_2, which shows that after the coating treatment, the Al powder had a characteristic diffraction peak in the form of a circular mound between 20 and 30°, indicating the presence of amorphous SiO_2 in the Al powder particles. Figure 1c shows the XPS spectrum of Al@SiO_2, which indicates that the SiO_2-coated Al powder has a signal peak of Si 2p and the corresponding position of the outgoing peak is 103.5 eV. Therefore, the presence of SiO_2 in the Al powder after the cladding treatment was further confirmed by the XPS spectra.

The FT-IR, XRD, and XPS results indicate the presence of SiO_2 in the cladding-treated Al powder particles and cannot directly indicate the generation of the core−shell microstructure. To see the Al@SiO_2 core−shell microstructure, the morphology of Al@SiO_2 was further observed by TEM. The results indicate that the sol−gel method does generate a distinct SiO_2 shell layer upon the surface of aluminum powder, and the SiO_2 shell layer thickness can be calculated based on the size of the Al powder particles and the scale bar. From Figure 2a,b, the SiO_2 shell layer thickness is ∼10 nm. Figure 2c,d show the elemental distribution and EDS energy spectrum analysis of the core−shell filler, respectively. These results demonstrate the presence of SiO_2 in the Al powder particles after the cladding treatment and verify the presence of SiO_2 on the Al powder surface, suggesting the formation of the Al@SiO_2 core−shell microstructure.

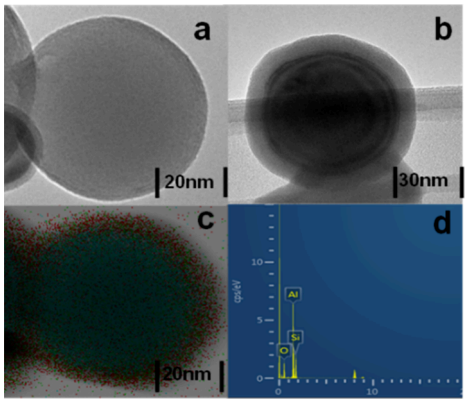

Figure 2. (a) TEM images of Al, (b) TEM of Al@SiO_2, (c) Element distribution of Al@SiO_2, (d) EDS spectrum of Al@SiO_2.

3.2. Regulation of Al@SiO_2 Core−Shell Packing Thickness. TEM was utilized to investigate the thickness of the SiO_2 layer, which can be adjusted by altering the initial tetraethyl orthosilicate (TEOS) concentration. Figure 3a shows that with the progressively increasing of the feeding SiO_2/Al mass ratio, the shell layer thickness gradually increases, reaching a maximum of about 22 nm at the feeding SiO_2/Al mass ratio of 0.8. Then, with the feeding SiO_2/Al mass ratio increasing, the SiO_2 shell layer thickness decreases probably because the excessive TEOS self-core formation of SiO_2 affects the coating of SiO_2 on the Al powder surface. The thickness of the SiO_2 shell layer can also be controlled by varying the reaction time. As depicted in Figure 3b, the shell layer thickness of Al@SiO_2 particles gradually increases with prolonged TEOS hydrolysis reaction time before eventually reaching a plateau. This indicates that it takes some time for TEOS to react with the surface of the Al powder and form a stable SiO_2 shell layer. Additionally, it was observed that the thickness of the shell layer on the Al@SiO_2 core−shell particles remains uniform and stable after a reaction time of 3 h. Thus, evidently, the cladding thickness of the Al@SiO_2 particles is influenced by both the TEOS feeding concentration and reaction time. The stable and adjustable Al@SiO_2 core−shell particles were obtained by controlling these two parameters.

3.3. Room Temperature Dielectric Properties of Silicone/Al@SiO_2 Core−Shell Fillers. Thin sheets were created from the Al@SiO_2 core−shell particles by using a press, and the dielectric properties of the resulting solid powder were evaluated over a frequency range of 10^{-1}−10^6 Hz. Figure 4a illustrates that as the thickness of the shell layer on the core−shell filler increases, the dielectric constant of the powder decreases. This result is reasonable because according to the effective dielectric theory, as the shell thickness increase, the volume fraction of silica increases, and the dielectric constant decrease.[31,32] Figure 4b,c show the trend of ε' and ε'' for the same core−shell filler content and different shell thicknesses in silicone. The composites with thin shell filler exhibit higher dielectric constants and lower dielectric losses over all the tested frequency, indicates the thin shell filler leading to better dielectric performance.

The dielectric properties of HTV/Al@SiO_2 silicone rubber composites were investigated at 25 °C, with a focus on the relationship between the dielectric constant and frequency. Measurements were taken across the range of 10^{-1}−10^6 Hz and the results are shown in Figure 5. It was found that for a given amount of added core−shell filler the permittivity of the silicone rubber composites was higher than that of a composite made with metallic Al and silicone rubber. In addition, the greater the amount of core−shell filler added, the higher the resulting permittivity of the composite. As the frequency increased, the dielectric constant of composites with core−shell fillers decreased, with a greater drop observed at higher core−shell filler content. This can be attributed to the strong interaction between the core−shell filler and the matrix, resulting in more pronounced interfacial polarization.[33]

The effect of core−shell filler addition was also shown to influence the dielectric loss. Figure 5b shows that the dielectric loss of the composite containing metallic Al powder decreased exponentially with the increase in frequency at low frequencies, which indicates DC conductance. The composites with core−shell fillers showed no such change and instead, a loss peak appeared. In addition, for the same core−shell filler, the higher filler content leads to higher dielectric loss of the materials. The DC conductance of the composite of silicone rubber and metallic Al powder at low frequencies can also be demonstrated from the plateau in Figure 5c. Under the same added filler mass, the electrical breakdown strength of the silicone−core−shell filler composite is higher than that of the silicone-metallic Al composite. For the same core−shell filler, the higher is the amount of added filler, the lower is the

https://doi.org/10.1021/acsomega.3c05066
ACS Omega 2023, 8, 35275−35282

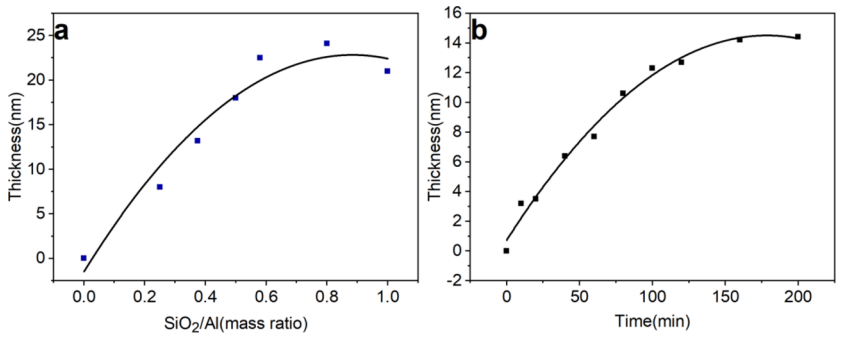

Figure 3. (a) The relationship between the thickness of Al@SiO_2 and the silicon to aluminum ratio; (b) Thickness of Al@SiO_2 as a function of reaction time.

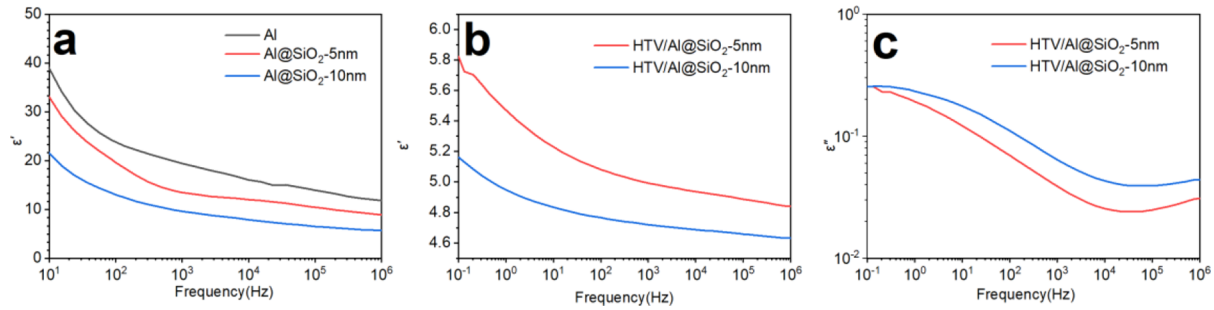

Figure 4. (a) ε' of Al@SiO_2 with different thicknesses; (b) ε' of HTV/Al@SiO_2 with different thicknesses; (c) ε'' of HTV/Al@SiO_2 with different thicknesses.

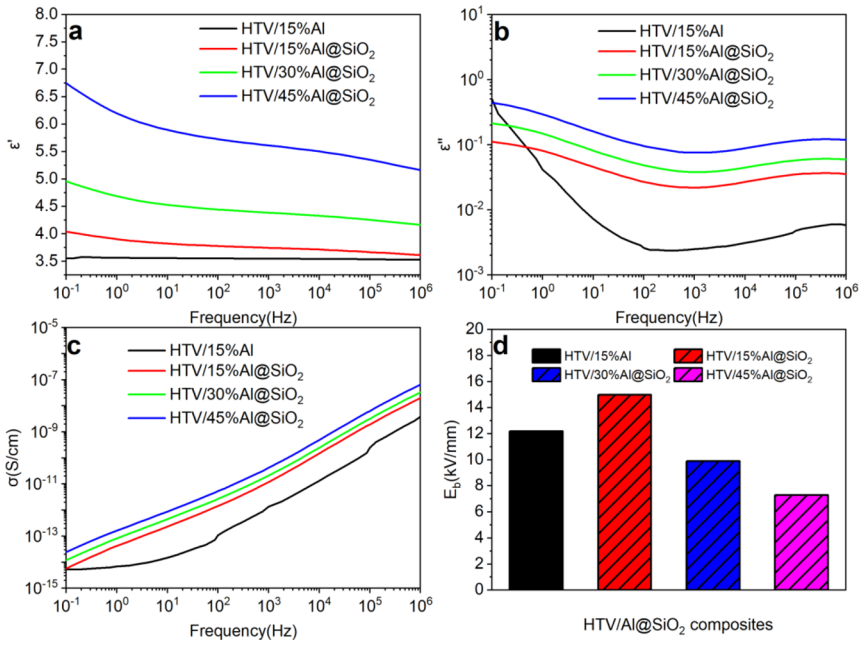

Figure 5. Dielectric properties of HTV/Al@SiO_2 composites. (a) Permittivity ε', (b) dielectric loss ε'', (c) conductivity σ, (d) electrical breakdown strength E_b.

electrical breakdown strength (E_b) of the composite, for example, the E_b decrease to 1.45 kV/mm as the Al@SiO_2 increase to 150% (Table 1).

3.4. Temperature Dependence of Dielectric Performance of Silicone/Al@SiO_2 Composites. The dielectric characteristics of the materials exhibit notable fluctuations with temperature because of the effect of heat on the dipoles.[34] Yet, when a specific external electric field is introduced, the dipoles tend to arrange in a directional manner and align themselves with the direction of the external electric field.[35]

Figure 6a illustrates a noticeable α relaxation in the composite at low temperatures. The ε' of the composite presents a distinct peak at approximately −90 °C, regardless of the filler used. Figure 6b demonstrates that the α relaxation of HTV/Al@SiO_2 is suitable for all frequencies. The peak of the α relaxation decreases as the frequency increases, which may be due to the reduction in the number of dipoles arranged

https://doi.org/10.1021/acsomega.3c05066
ACS Omega 2023, 8, 35275−35282

Table 1. Dielectric Properties of the HTV/Al@SiO_2 Composites

	ε' (1 kHz)	ε''(1 kHz)	tan δ (1 kHz)	σ (S/cm) (1 kHz)	E_b (kV/mm)
HTV/15%Al	3.52	2.49×10^{-3}	9.08×10^{-4}	1.34×10^{-12}	12.20
HTV/15%Al@SiO_2	3.74	2.20×10^{-2}	5.75×10^{-3}	1.20×10^{-11}	15.00
HTV/30%Al@SiO_2	4.41	3.80×10^{-2}	8.67×10^{-3}	2.12×10^{-11}	9.90
HTV/45%Al@SiO_2	5.62	7.53×10^{-2}	1.34×10^{-2}	4.19×10^{-11}	7.30
HTV/100%Al@SiO_2	14.34	2.64×10^{-1}	1.85×10^{-2}	1.70×10^{-10}	2.10
HTV/150%Al@SiO_2	17.03	3.79×10^{-1}	2.24×10^{-2}	2.43×10^{-10}	1.45

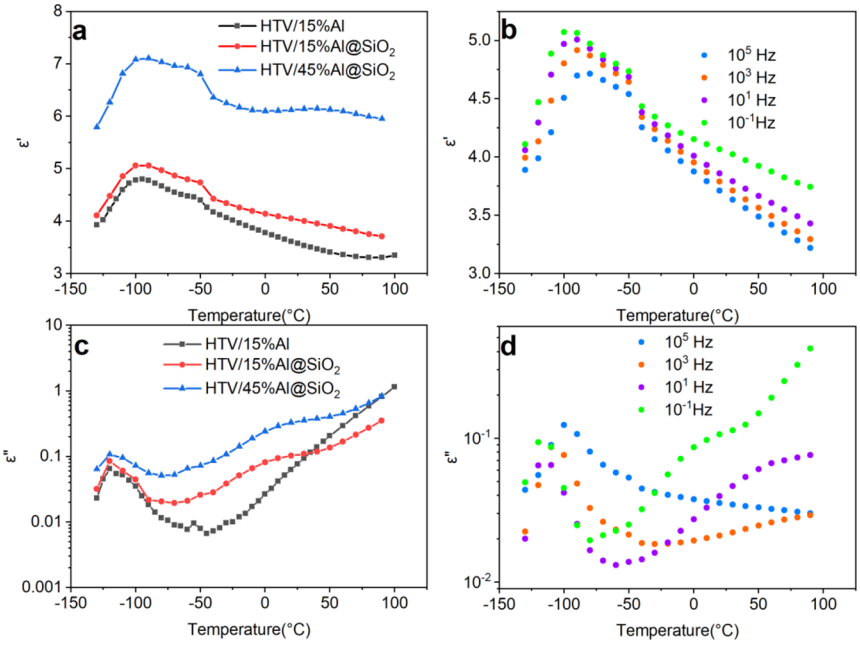

Figure 6. Dielectric properties of HTV/Al@SiO_2 composites exhibit a temperature dependence. The variation of ε' with temperature is presented in (a) for HTV/Al@SiO_2 (0.1 Hz) and in (b) for HTV/15%Al@SiO_2 at different frequencies. The temperature dependence of ε'' is shown in (c) for HTV/Al@SiO_2 (0.1 Hz) and in (d) for HTV/15%Al@SiO_2 at different frequencies.

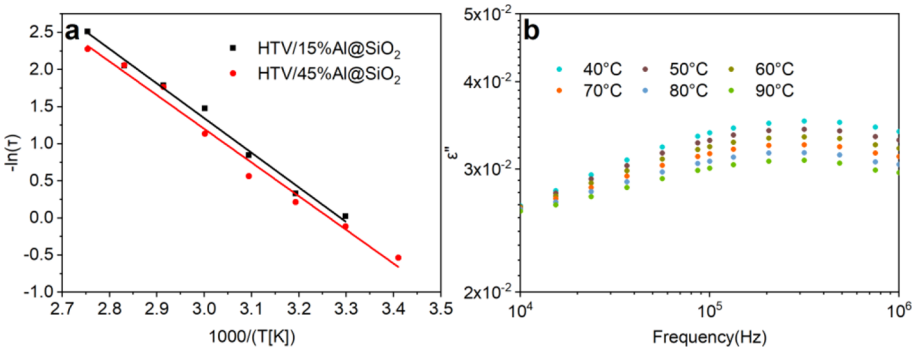

Figure 7. (a) An activation plot was generated for the relaxation time of MWS relaxation in HTV/Al@SiO_2; (b) The MWS-relaxation process of HTV/15% Al@SiO_2 was examined.

under the applied electric field.[36] The significant increase in ε' of the composite at higher temperatures and lower frequencies can be attributed to interface polarization.[37] Figure 6c shows that the ε'' of the composite has a sharp peak at approximately −120 °C, which is not influenced by the type or amount of filler. When the temperature range above the T_g, as the temperature increases, the ε'' of HTV/Al@SiO_2 exhibits a significant loss peak, while the ε'' of HTV/Al does not have this loss peak. This is attributed to the interface interactions of core−shell filler and silicon.[38] The interfacial polarization is caused by the strong interactions within the rubber matrix.[39] HTV/Al@SiO_2 and HTV/Al exhibited significant DC conductance with increasing temperature. However, compared to the metallic Al powder, adding core−shell fillers had an inhibitory effect on the DC conductance. Figure 6d indicates that the ε'' of the composite demonstrated similar temperature dependence at various test frequencies. The α-relaxation and interfacial relaxation occurred shifted toward higher temperatures as the frequency rose. The peaks for α-relaxation and interfacial relaxation decreased and vanished within the observable frequency and temperature range.

https://doi.org/10.1021/acsomega.3c05066
ACS Omega 2023, 8, 35275−35282

3.5. Dielectric Relaxation Behavior of Silicone Rubber/Al@SiO_2 Core−Shell Filler. To further explore the influence of core−shell fillers on the dielectric relaxation behavior of silicone composites, the study examined the impact of HTV/Al@SiO_2 on interfacial polarization and DC conductance relative to HTV/Al. The imaginary part of the dielectric constant (ε'') was analyzed using the Havriliak−Negami equation[40] at different temperatures to assess the dielectric response behavior of the composite material. Subsequently, the relaxation behavior of the composite was analyzed to obtain the corresponding relaxation parameters.

HTV/Al@SiO_2 displays distinct MWS relaxation above T_g, as compared to HTV/Al. While there is a conductance contribution in the higher temperature range, its DC conductance is not predominant. Fitted by Havriliak−Negami model, the relaxation times for various relaxation peaks at different temperatures can be identified. It is observed that the relaxation time is sensitive to temperature as the dipole movement tends to accelerate with a rise in temperature.[41] Furthermore, the temperature dependence of the relaxation time can be utilized to determine the activation energy (E_a).

The relaxation at the HTV/Al@SiO_2 interface is primarily ascribed to the interface formed between the polymer chain and the core−shell filler. Figure 7a indicates that the interfacial MWS relaxation times of both composites comply with the Arrhenius equation.[42]

$$\tau = \tau_0 \exp\left(\frac{E_a}{kT}\right) \quad (1)$$

Table 2 shows the fitted Arrhenius parameters. The dielectric relaxation strength of MWS relaxation increases with temperature, and the interface polarization peak shifts toward higher frequencies.[43] The dielectric relaxation strength of the composite material increases with the addition of a core−shell filler. The apparent activation energies for the MWS relaxation of HTV/15%Al@SiO_2 and HTV/45%Al@SiO_2 are 38.83 and 37.75 kJ/mol, respectively, which are not significantly different.

Table 2. Relationship between Temperature and Relaxation Time, as Well as DC Conductance, in Composites of HTV/Al@SiO_2

	MWS relaxation		DC conductance	
	ln τ_0 (s)	E_a (kJ/mol)	ln σ_0 (S/cm)	E_a (kJ/mol)
HTV/15%Al	-	-	−17.51	38.91
HTV/15%Al@SiO_2	−15.34	38.83	−11.65	61.19
HTV/45%Al@SiO_2	−14.81	37.75	−12.37	55.29

The impact of the conductance on the dielectric loss spectrum was examined. As depicted in Figure 8, the composite material displayed substantial conductance polarization in the high temperature range. Nevertheless, incorporating core−shell fillers hindered or delayed the onset of DC conductance. The greater the amount of core−shell filler added, the more pronounced the inhibition. The temperature-dependent behavior of DC conductance followed the Arrhenius equation is as expressed below:[44]

$$\sigma = \sigma_0 \exp\left(\frac{E_a}{kT}\right) \quad (2)$$

According to Table S2, the exponential factor of the DC conductance for the HTV/Al composites ($0.85 < N < 1$) is considerably greater than that of the HTV/Al@SiO_2 composites ($N < 0.65$). This suggests that DC conductance does not play a dominant role in the relaxation process of the HTV/Al@SiO_2 composite in the high-temperature and low-frequency range.[45] Moreover, as the proportion of the core−shell filler increases, its ability to inhibit DC conductance in the composite becomes more apparent.

The apparent E_a of DC conductance in composites containing core−shell fillers is notably higher than that in those containing metallic Al powders. The addition of HTV/45%Al@SiO_2 results in an E_a of 55.29 kJ/mol, while the addition of HTV/15%Al@SiO_2 yields an E_a of 61.19 kJ/mol, both significantly larger than the apparent E_a of HTV/Al (38.91 kJ/mol). In addition, Table 2 demonstrates that incorporating core−shell fillers increases the σ_0 values of the composites.

4. CONCLUSIONS

Using the sol−gel method, a SiO_2 shell layer was successfully applied onto the surface of metallic aluminum powder, resulting in the creation of an Al@SiO_2 core−shell filler. By adjustment of the feeding TEOS concentration and reaction time, the thickness of the Al@SiO_2 shell layer can be precisely controlled. In comparison to HTV/Al composites of the same filling amount, the dielectric constants of HTV/Al@SiO_2 composites were found to be higher. At high frequencies, the dielectric loss of HTV/Al@SiO_2 composites was greater, while at low frequencies, it was smaller, when compared to that of

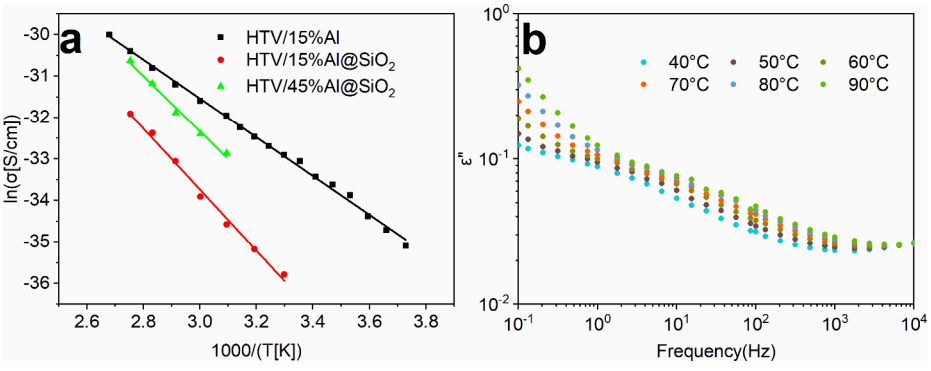

Figure 8. (a) The relaxation time of DC conductance in HTV/Al@SiO_2 can be represented by an activation plot. (b) DC conductance process of HTV/15% Al@SiO_2 can be depicted.

https://doi.org/10.1021/acsomega.3c05066
ACS Omega 2023, 8, 35275−35282

HTV/Al composites. In addition, the electrical breakdown strength of the HTV/Al@SiO_2 composites was greater than that of the HTV/Al composites. Furthermore, the dielectric constant and dielectric loss of the composite increased with the increase in Al@SiO_2 core−shell filler. Comparatively, the prepared Al@SiO_2 core−shell filler enhances the contribution of the MWS relaxation in composite material and restrains the contribution of its DC conductance, when compared to aluminum nanopowder.

■ ASSOCIATED CONTENT

Supporting Information

The Supporting Information is available free of charge at https://pubs.acs.org/doi/10.1021/acsomega.3c05066.

Data models and analysis methods, additional dielectric performance (PDF)

■ AUTHOR INFORMATION

Corresponding Authors

Zhijie Zhang − *Key Laboratory of Science and Technology on High-Tech Polymer Materials, Institute of Chemistry, Chinese Academy of Sciences, Beijing 100190, P. R. China*; Email: zhangzj@iccas.ac.cn

Hua-Feng Fei − *Key Laboratory of Science and Technology on High-Tech Polymer Materials, Institute of Chemistry, Chinese Academy of Sciences, Beijing 100190, P. R. China; School of Chemical Sciences, University of Chinese Academy of Sciences, Beijing 100049, P. R. China*; orcid.org/0000-0002-9983-2725; Email: feihuafeng@iccas.ac.cn

Authors

Bin Huang − *Key Laboratory of Science and Technology on High-Tech Polymer Materials, Institute of Chemistry, Chinese Academy of Sciences, Beijing 100190, P. R. China*

Yan Yu − *Key Laboratory of Science and Technology on High-Tech Polymer Materials, Institute of Chemistry, Chinese Academy of Sciences, Beijing 100190, P. R. China; School of Chemical Sciences, University of Chinese Academy of Sciences, Beijing 100049, P. R. China*

Yan Zhao − *Key Laboratory of Science and Technology on High-Tech Polymer Materials, Institute of Chemistry, Chinese Academy of Sciences, Beijing 100190, P. R. China; School of Chemical Sciences, University of Chinese Academy of Sciences, Beijing 100049, P. R. China*

Yunfeng Zhao − *Key Laboratory of Science and Technology on High-Tech Polymer Materials, Institute of Chemistry, Chinese Academy of Sciences, Beijing 100190, P. R. China*

Lina Dai − *Key Laboratory of Science and Technology on High-Tech Polymer Materials, Institute of Chemistry, Chinese Academy of Sciences, Beijing 100190, P. R. China*

Complete contact information is available at: https://pubs.acs.org/10.1021/acsomega.3c05066

Notes

The authors declare no competing financial interest.

■ ACKNOWLEDGMENTS

The facilities used in this work were supported by the Analytical Instrumental Center for Physicochemical Analysis and Measurements, affiliated with the Chinese Academy of Sciences.

■ REFERENCES

(1) Seo, J.; Kim, D.; Hwang, S.; Shim, S. E. A Review on Recent Development and Applications of Dielectric Elastomers. *Elastomers Compos.* **2021**, *56*, 57−64.

(2) Qiu, Y.; Zhang, E.; Plamthottam, R.; Pei, Q. Dielectric Elastomer Artificial Muscle: Materials Innovations and Device Explorations. *Acc. Chem. Res.* **2019**, *52*, 316−325.

(3) Wang, N. F.; Cui, C. Y.; Guo, H.; Chen, B. C.; Zhang, X. M. Advances in dielectric elastomer actuation technology. *Sci. China Technol. Sci.* **2018**, *61*, 1512−1527.

(4) Tingting, L.; Qian, L.; Sanfa, X. Research Progress of Dielectric Elastomers. *Polym. Bull.* **2018**, 10−18.

(5) Madsen, F. B.; Daugaard, A. E.; Hvilsted, S.; Skov, A. L. The Current State of Silicone-Based Dielectric Elastomer Transducers. *Macromol. Rapid Commun.* **2016**, *37*, 378−413.

(6) Zhu, F.; Zhang, C.; Qian, J.; Chen, W. Mechanics of dielectric elastomers: materials, structures, and devices. *J. Zhejiang Univ., Sci. A* **2016**, *17*, 1−21.

(7) Romasanta, L. J.; Lopez-Manchado, M. A.; Verdejo, R. Increasing the performance of dielectric elastomer actuators: A review from the materials perspective. *Prog. Polym. Sci.* **2015**, *51*, 188−211.

(8) Skov, A. L.; Yu, L. Optimization Techniques for Improving the Performance of Silicone-Based Dielectric Elastomers. *Adv. Eng. Mater.* **2018**, *20*, No. 1700762.

(9) Dünki, S. J.; Nüesch, F. A.; Opris, D. M. Elastomers with tunable dielectric and electromechanical properties. *J. Mater. Chem. C* **2016**, *4*, 10545−10553.

(10) Sun, H.; Liu, X.; Yu, B.; Feng, Z.; Ning, N.; Hu, G.-H.; Tian, M.; Zhang, L. Simultaneously improved dielectric and mechanical properties of silicone elastomer by designing a dual crosslinking network. *Polym. Chem.* **2019**, *10*, 633−645.

(11) Yu, Y.; Huang, B.; Zhao, Y.; Zhao, Y.; Dai, L.; Zhang, Z.; Fei, H.-F. Enhanced Dielectric Properties of Polydimethylsiloxane Elastomer-Based Composites with Cyanosilicone. *ACS Appl. Polym. Mater.* **2023**, *5*, 259−268.

(12) Yu, Y.; Zhao, Y.; Huang, B.; Ji, Y.; Zhao, Y.; Zhang, Z.; Fei, H.-F. Dielectric properties and dielectric relaxation process of polymethylphenylsiloxane/silicon dioxide nanocomposites. *J. Appl. Polym. Sci.* **2022**, *139*, No. e52716.

(13) Vaimakis-Tsogkas, D. T.; Bekas, D. G.; Giannakopoulou, T.; Todorova, N.; Paipetis, A. S.; Barkoula, N.-M. Effect of TiO2 addition/coating on the performance of polydimethylsiloxane-based silicone elastomers for outdoor applications. *Mater. Chem. Phys.* **2019**, *223*, 366−373.

(14) Kim, T.; Lim, H.; Lee, Y.; Kim, B.-J. Synthesis of BaTiO3 nanoparticles as shape modified filler for high dielectric constant ceramic−polymer composite. *RSC Adv.* **2020**, *10*, 29278−29286.

(15) Zhang, Y.-Y.; Min, Y.; Wang, G.-L.; Wang, Z.-F.; Liu, J.-L.; Luo, Z.-W.; Zhang, M. Design and properties of calcium copper titanate/poly(dimethyl siloxane) dielectric elastomer composites. *Rare Met.* **2021**, *40*, 2627−2632.

(16) Zeng, Y.; Zhou, N.; Xiong, C.; Huang, Z.; Du, G.; Fan, Z.; Chen, N. Highly stretchable silicone rubber nanocomposites incorporated with oleic acid-modified Fe3O4 nanoparticles. *J. Appl. Polym. Sci.* **2022**, *139*, 51476.

(17) Liu, X.; Sun, H.; Liu, S.; Jiang, Y.; Yin, Z.; Yu, B.; Ning, N.; Tian, M.; Zhang, L. Dielectric elastomer sensor with high dielectric constant and capacitive strain sensing properties by designing polar-nonpolar fluorosilicone multiblock copolymers and introducing poly(dopamine) modified CNTs. *Composites, Part B* **2021**, *223*, No. 109103.

(18) Cai, C.; Chen, T.; Chen, X.; Zhang, Y.; Gong, X.; Wu, C.; Hu, T. Enhanced Electromechanical Properties of Three-Phased Polydimethylsiloxane Nanocomposites via Surface Encapsulation of Barium Titanate and Multiwalled Carbon Nanotube with Polydopamine. *Macromol. Mater. Eng.* **2021**, *306*, No. 2100046.

(19) Krisnadi, F.; Nguyen, L. L.; Ankit, J.; Ma, J.; Kulkarni, M. R.; Mathews, N.; Dickey, M. D. Directed Assembly of Liquid Metal−

Elastomer Conductors for Stretchable and Self-Healing Electronics. *Adv. Mater.* **2020**, *32*, No. 2001642.
(20) Racles, C.; Dascalu, M.; Bele, A.; Tiron, V.; Asandulesa, M.; Tugui, C.; Vasiliu, A.-L.; Cazacu, M. All-silicone elastic composites with counter-intuitive piezoelectric response, designed for electromechanical applications. *J. Mater. Chem. C* **2017**, *5*, 6997−7010.
(21) Madsen, F. B.; Yu, L.; Mazurek, P.; Skov, A. L. A simple method for reducing inevitable dielectric loss in high-permittivity dielectric elastomers. *Smart Mater. Struct.* **2016**, *25*, No. 075018.
(22) Fei, L.; Zijing, Z.; Lingyan, S.; Chonggang, W.; Xinghou, G.; Gang, S.; Tao, H. Advance in dielectric elastomer based on inorganic particle filled silicone rubber. *New Chem. Mater.* **2019**, *47* (33−37), 45.
(23) Shankar, B. S. M.; Kulkarni, S. M. Influences of dielectric and conductive fillers on dielectric and mechanical properties of solid silicone rubber composites, Iran. *Polym. J.* **2019**, *28*, 563−573.
(24) Banet, P.; Zeggai, N.; Chavanne, J.; Nguyen, G. T. M.; Chikh, L.; Plesse, C.; Almanza, M.; Martinez, T.; Civet, Y.; Perriard, Y.; Fichet, O. Evaluation of dielectric elastomers to develop materials suitable for actuation. *Soft Matter* **2021**, *17*, 10786−10805.
(25) Zhou, Z.; Wang, H.; Zhu, Z.; Yang, H.; Zhang, Q. Enhanced dielectric, electromechanical and hydrophobic behaviors of core-shell AgNWs@SiO2/PDMS composites. *Colloids Surf., A* **2019**, *563*, 59−67.
(26) Liu, L.; Lei, Y.; Zhang, Z.; Liu, J.; Lv, S.; Guo, Z. Fabrication of PDA@SiO2@rGO/PDMS dielectric elastomer composites with good electromechanical properties. *React. Funct. Polym.* **2020**, *154*, No. 104656.
(27) Sadroddini, M.; Razzaghi-Kashani, M. Silica-decorated reduced graphene oxide (SiO2@rGO) as hybrid fillers for enhanced dielectric and actuation behavior of polydimethylsiloxane composites. *Smart Mater. Struct.* **2020**, *29*, No. 015028.
(28) Quinsaat, J. E. Q.; Alexandru, M.; Nüesch, F. A.; Hofmann, H.; Borgschulte, A.; Opris, D. M. Highly stretchable dielectric elastomer composites containing high volume fractions of silver nanoparticles. *J. Mater. Chem. A* **2015**, *3*, 14675−14685.
(29) Zhang, J.; Zhao, F.; Zuo, Y.; Zhang, Y.; Chen, X.; Li, B.; Zhang, N.; Niu, G.; Ren, W.; Ye, Z. Improving actuation strain and breakdown strength of dielectric elastomers using core-shell structured CNT-Al2O3. *Compos. Sci. Technol.* **2020**, *200*, No. 108393.
(30) Yang, Y.; Tao, J.-R.; Yang, D.; He, Q.-M.; Chen, X.-D.; Wang, M. Improving dispersion and delamination of graphite in biodegradable starch materials via constructing cation-π interaction: Towards microwave shielding enhancement. *J. Mater. Sci. Technol.* **2022**, *129*, 196.
(31) Quinsaat, J. E. Q.; Nüesch, F. A.; Hofmann, H.; Opris, D. M. Dielectric properties of silver nanoparticles coated with silica shells of different thicknesses. *RSC Adv.* **2013**, *3*, 6964.
(32) Tao, J.-R.; Yang, D.; Yang, Y.; He, Q.-M.; Fei, B.; Wang, M. Migration mechanism of carbon nanotubes and matching viscosity-dependent morphology in Co-continuous Poly(lactic acid)/Poly(ε-caprolactone) blend: Towards electromagnetic shielding enhancement. *Polymer* **2022**, *252*, No. 124963.
(33) Xiong, L.; Zheng, S.; Xu, Z.; Liu, Z.; Yang, W.; Yang, M. Enhanced performance of porous silicone-based dielectric elastomeric composites by low filler content of Ag@SiO2 Core-Shell nanoparticles. *Nanocomposites* **2018**, *4*, 238−243.
(34) Huang, B.; Yu, Y.; Zhao, Y.; Zhao, Y.; Dai, L.; Zhang, Z.; Fei, H.-F. Efficient self-repairing high permittivity cyanosilicone dielectric elastomers. *Polymer* **2023**, *280*, No. 126047.
(35) Nayak, S.; Chaki, T. K.; Khastgir, D. Development of Flexible Piezoelectric Poly(dimethylsiloxane)−BaTiO3 Nanocomposites for Electrical Energy Harvesting. *Ind. Eng. Chem. Res.* **2014**, *53*, 14982−14992.
(36) Lotonov, A. M.; Gavrilova, N. D.; Kramarenko, E. Y.; Alekseeva, E. I.; Popov, P. Y.; Stepanov, G. V. Effect of iron particles on dielectric properties of polydimethylsiloxane near crystallization and glass transition temperatures. *Polym. Sci. Ser., B* **2006**, *48*, 267−270.
(37) Lestriez, B.; Maazouz, A.; Gerard, J. F.; Sautereau, H.; Boiteux, G.; Seytre, G.; Kranbuehl, D. E. Is the Maxwell−Sillars−Wagner model reliable for describing the dielectric properties of a core−shell particle−epoxy system? *Polymer* **1998**, *39*, 6733−6742.
(38) Aboubakr, S.; Rguiti, M.; Yessari, M.; Elballouti, A.; Courtois, C.; Hajjaji, A. Dielectric characterization of lead zirconate-titane-(PZT) /polyurethane(PU) thin film composite: Volume fraction, frequency and temperature dependence. *Mol. Cryst. Liq. Cryst.* **2016**, *627*, 82−91.
(39) Klonos, P.; Kyritsis, A.; Bokobza, L.; Gunko, V. M.; Pissis, P. Interfacial effects in PDMS/titania nanocomposites studied by thermal and dielectric techniques. *Colloids Surf., A* **2017**, *519*, 212−222.
(40) Chen, C.; Sun, Q.; Wang, C.; Bu, Y.; Zhang, J.; Peng, Z. Dielectric Relaxation Characteristics of Epoxy Resin Modified with Hydroxyl-Terminated Nitrile Rubber. *Molecules* **2020**, *25*, 4128.
(41) Paluch, M.; Roland, C. M.; Pawlus, S. Temperature and pressure dependence of the α-relaxation in polymethylphenylsiloxane. *J. Chem. Phys.* **2002**, *116*, 10932−10937.
(42) Kriegs, H.; Gapinski, J.; Meier, G.; Paluch, M.; Pawlus, S.; Patkowski, A. Pressure effects on the α and α' relaxations in polymethylphenylsiloxane. *J. Chem. Phys.* **2006**, *124*, 104901.
(43) Yu, Y.; Zhao, Y.; Huang, B.; Ji, Y.; Zhao, Y.; Zhang, Z.; Fei, H.-F. Effect of phenyl side groups on the dielectric properties and dielectric behavior of polysiloxane. *Polymer* **2022**, *249*, No. 124865.
(44) Kareem, A. A. Thermal and electrical properties of polyimide/PANI nanofiber composites prepared via in situ polymerization. *Mater. Sci. Poland* **2018**, *36*, 283−287.
(45) Panda, S.; Goswami, S.; Acharya, B. Polydimethylsiloxane-Multiwalled Carbon Nanotube Nanocomposites as Dielectric Materials: Frequency, Concentration, and Temperature-Dependence Studies. *J. Elecron. Mater.* **2019**, *48*, 2853−2864.

https://doi.org/10.1021/acsomega.3c05066
ACS Omega 2023, 8, 35275−35282